Desalination and Water Treatment
www.deswater.com
doi: 10.5004/dwt.2020.26063

200 (2020) 23–41
October

Analysis of transfer functions and normalizations in an ANN model that predicts the transport of energy in a parabolic trough solar collector

E.D. Reyes-Téllez[a], A. Parrales[b,*], G.E. Ramírez-Ramos[a], J.A. Hernández[c,*], G. Urquiza[c], M.I. Heredia[a], F.Z. Sierra[c]

[a]*Posgrado – Centro de Investigación en Ingeniería y Ciencias Aplicadas (CIICAp), Universidad Autónoma del Estado de Morelos, Av. Universidad 1001, Col. Chamilpa, C.P. 62209, Cuernavaca, Morelos, México, Tel. +527773297084; emails: das_sb@hotmail.com (E.D. Reyes-Téllez), gidy22@gmail.com (G.E. Ramírez-Ramos), miguel.heredia@uaem.mx (M.I. Heredia)*
[b]*CONACyT – Centro de Investigación en Ingeniería y Ciencias Aplicadas (CIICAp), Universidad Autónoma del Estado de Morelos, Av. Universidad 1001, Col. Chamilpa, C.P. 62209, Cuernavaca, Morelos, México, email: arianna.parrales@uaem.mx (A. Parrales)*
[c]*Centro de Investigación en Ingeniería y Ciencias Aplicadas (CIICAp), Universidad Autónoma del Estado de Morelos(UAEM), Av. Universidad 1001, Col. Chamilpa, C.P. 62209, Cuernavaca, Morelos, México, emails: alfredo@uaem.mx (J.A. Hernández), gurquiza@uaem.mx (G. Urquiza), fse@uaem.mx (F.Z. Sierra)*

Received 4 December 2019; Accepted 2 May 2020

ABSTRACT

Artificial neural network model was developed to obtain the fluid outlet temperature of the parabolic trough collector (PTC) with a grooved absorber tube. To improve the accuracy of the model, an analysis of the transfer functions was performed at different normalization intervals to choose the best model capable of estimating the PTC outlet temperature. A first model was developed that was used as a base model from 1,155 concordant experimental data. The variables were input temperature of the fluid, ambient temperature, irradiance, hour, day, configuration, volumetric flow, feeding temperature, and storage temperature. To validate the accuracy and the adaptability of the model proposed, statistical tests (coefficient of determination (R^2), root mean square error (RMSE), and mean absolute percent error (MAPE), significance test (F-Fisher and t-student), and linearity test (slope-intercept)) were performed. The base model was validated, having an R^2 = 0.9961, RMSE = 0.14706, MAPE = 0.00795, also approved significance and linearity tests. Consequently, ten models were developed for the analysis of the proposed normalization intervals using the same architecture as the base model at five areas of interest with a hyperbolic tangent sigmoid (TANSIG) and log-sigmoid (LOGISIG) functions. The results show that a model has higher accuracy; this model was the TANSIG of [0.1,0.9] with R^2 = 0.9974, RMSE = 0.12123, MAPE = 5.93×10^{-5}, and approved significance and linearity.

Keywords: Parabolic trough solar collector; Artificial neural network; Normalization; Transfer function; Linearity test

1. Introduction

To reduce the environmental consequences by use of energy coming from the consumption of fossil fuels, the majority of countries and their researchers have promoted the use of renewable energies [1]. Among all the energies source considered renewable, solar energy is the cleanest energy with high potential and a possible sustainable alternative that could satisfy global energy demand [2], taking into account that it needs to be collected and stored efficiently [3]. One

* Corresponding authors.

way to take advantage of the Sun's energy is through solar thermal collectors STC, whose exists several types depending on its application and design.

Solar thermal collectors are a particular type of heat exchangers used to absorb incoming solar radiation, transforming it into heat, and then transfer it to a working fluid. Are mainly classified into two types according to the concentration ratio: concentrated and non-concentrated [4]. Within the classification of solar concentrating collectors, the parabolic trough solar collector parabolic trough collector (PTC) stands out due to its wide acceptance angle, a high capacity to take advantage of diffuse light, and low cost. PTCs have a wide range of thermal availability that allows meeting the heat energy requirements of some industrial processes or electric power generation [5].

The PTC uses a parabolic reflector to concentrate the incident sun rays along a focal line in which an absorber tube is placed. The PTC's primary function is to transform the solar radiation and convert it to thermal energy through increasing the temperature of a heat transfer fluid that circulates into the absorber tube. Then, the thermal energy collected is stored or used in some processes. Generally, the absorber tube has a selective coating to decrease the emittance and reduce thermal losses [6].

Moreover, through active or passive techniques, the energy absorbed in the tube can increase. On one side, the active techniques require an external energy source, and their use is limited due to the difficulties of implementing them. On the other hand, passive techniques are simple and less expensive [7]. These consist of changing or increasing the heat exchange surface employing fins, braided inserts, corrugations, grooves, among others [8]. The grooved tubes or with internal fins have better thermo-hydraulic performance due to their higher heat transfer coefficient with lower pressure loss compared to twisted inserts, corrugated pipes, or dimpled tubes [9].

In particular, grooved tubes are that have an arrangement of channels on the inner surface that can be as circular, rectangular, trapezoidal, or triangular geometry [10]. These grooves generate turbulence and mixing in the flow in addition to periodic interruptions of the boundary layer, which improves the transfer of heat by forced convection. Therefore, to increase the thermal performance of the PTC system, grooves are a viable option to consider because of their effortless design, low cost, and high thermo-hydraulic performance depending on the geometry or size of the groove.

In regard to the thermal efficiency of the PTC system, numerous researches have been focused on understanding how the different operating parameters affect the amount absorbed of concentrated solar radiation within the receiver. Given that, the experiments are constrained by the processing time and operating costs [11], studies have been inclined towards the use of empirical models to describe the phenomenon with high accuracy and whit it replaces some experiments.

One of the most used tools in empirical modeling of non-linear phenomena has been the artificial neural networks (ANN) [12]. Specifically, the data coming from renewable energy systems are good candidates to be managed with ANN, since it is difficult to identify a precise mathematical function when some parameters vary by time and environmental factors [13]. Furthermore, Kalogirou [14] suggested that models based on ANN have demonstrated the effectiveness of its use in hypothetically designed solar collector systems.

ANN has been widely used to simulate solar collectors, as in the work of Sözen et al. [15], where he developed a new formula based on ANN to determine the efficiency of a flat plate solar collector with experimental data that were measured in July to September, obtaining a coefficient of determination of 0.983. The variables used in the input layer of the network were collector surface temperature, date, time, solar radiation, declination angle, azimuth angle, and tilt angle. The results were acceptable compared to the experimental data through statistical tests.

In a study developed by Caner et al. [16], an ANN model was created with eight normalized input variables between –1 and 1 to estimate the thermal performance of two air collectors. Experiments are carried out between 10:00–17:00 h in August and September. The statistical results of the comparisons between the predicted data and experimental data have been demonstrated the effectiveness of the proposed ANN.

In another work, Heng et al. [17] used ANNs with the superposition principle for transient thermal prediction in a PTC. The ANN model obtained was used to predict the temperature at the PTC output for a single pulse. The backpropagation network was trained with an architecture of three neurons in the input layer, two hidden layers with 68 neurons each one, and one neuron in the output layer. By gradient descent training algorithm with a total of 29,884 samples, an R^2 of 0.9999 was obtained. The input variables were heated flow, fluid velocity, and time.

On the other hand, the prediction of the performance parameters of flat-plate solar collectors by the use of ANN has been realized by Kalogirou [14]. In this work, with 6 ANN models developed, was obtained the prediction of the performance coefficients, both at the wind and no-wind conditions, the incidence angle, modifier coefficients at longitudinal and transverse directions, the collector time constant, the collector stagnation temperature and the collector heat capacity.

An ANN model was obtained by Reyes-Tellez et al. [18] to predict the hot-water outlet temperature of PTC with low-cost components. The best-fitting of training data was acquired with the architecture of nine neurons in the input layer, nine neurons in the hidden layer, and 1 in the output layer; considering a hyperbolic tangent sigmoid transfer function (TANSIG) in the hidden layer and a linear transfer function (PURELIN) in the output. Also, the combination of the inverse neural network coupled with genetic algorithms was used to predict the optimal operating conditions in a low-cost solar collector as a strategy to optimize the feeding tank temperature, being able to predict an exit temperature of up to 49°C from a supply temperature of 19°C. Additionally, May Tzuc et al. [19] developed a model to obtain the thermal efficiency of the PTC with a different normalization proposed. The model was achieved with an architecture of seven neurons in the input layer, three neurons in the hidden layer, and one neuron in the output layer; then, combining ANN with genetic algorithms, the optimal

water flow was estimated at the PTC array for a determined efficiency with errors below 2%.

The present work aimed to develop an accurate model based on ANN to determine the fluid outlet temperature in a parabolic trough solar collector, which used a tube grooved as an absorber tube. The accuracy model was carried out considering analyses on ten model ANN which applied different transfer functions as well as different normalizations. The main contributions of this work have been: (1) the development of a model based on ANN to determine the fluid outlet temperature of the PTC with an absorber grooved tube (2). The evaluation of different combinations of activation functions and normalizations to obtain an optimal model with the minimum error. The (3) statistical analysis to determine the model that had the best performance.

2. Description of experimental equipment

The PTC is a solar thermal concentrator, which is mainly consisting of a parabolic reflector 16-gauge type 316L stainless steel with mirror polishing on the inside. The concentrator consists of a vertically cut steel sheet drum with dimensions of 85 cm long by 57 cm in diameter. The receiver tube is made of a 1/2 inch long grooved copper tube and painted black to have a higher absorptivity. A second surface that is concentric to the receiver tube covers it externally and consists of two concentric glass tubes with different diameters. The characteristics of the PTC and the grooved absorber are shown in Table 1 and Fig. 1, respectively.

The PTC was instrumented with thermocouples type T duly calibrated for the measurement of temperature in the regions of interest: at the input of the grooved tube receiver (T_{input}), at the ambient (T_{amb}), at the tank of feeding or of cold water (T_{feed}), and at the hot water storage tank ($T_{storage}$). Likewise, it was registered the temperature at the outlet of the grooved receiver tube (T_{output}), which was the output variable or target for the ANN model. An Agilent 34970A card and the Agilent Benchlink Data Logger software were used to acquire and record experimental data.

The tanks of feeding and storage are 750 and 450 L, respectively. They are interconnected to have recirculation and thus raise the temperature of the feed tank when hot water is unused. Valves and a pressurizing motor pump model AQC-15 with a power of 2/15 HP were installed to control the flow. A Blue-White F-400 flowmeter with a capacity of 20 LPM was used to measure the volumetric flow at the outlet of the grooved tube.

2.1. Operating conditions

The PTC is located on the facilities of the CIICAp-UAEM Morelos [20], Mexico with latitude and longitude coordinates of 18.981655–99.23418, respectively. The PTC has an inclination of 19° and is oriented toward the East–West with the face of the reflecting plate pointing toward the South to better exploit the incidence of solar radiation. Fig. 2 shows a schematic diagram of the experimental system PTC with low-cost components.

As can be seen in Fig. 3, was realized four configurations in the PTC arrangement: (a) with glass cover that protects the PTC from the weather and dust, (b) without glass cover

Table 1
Geometric characteristics of the PTC experimental system

Variable	Value
Receptor length	0.85 m
Receptor internal diameter	0.0138 m
Receptor external diameter	0.0159 m
Internal diameter of the first cover	0.034 m
External diameter of the first cover	0.036 m
Internal diameter in of the second cover	0.048 m
External diameter of the second cover	0.05 m
Focal distance	0.025 m
Receptor absorbance	0.906
Receptor emittance	0.14
Glass cover transmittance	0.95
Reflectivity surface	0.93
Shape factor	0.92
Tilt angle	18.5°
Incident angle modifier	1
Optical efficiency	0.56
Glass cover emittance	0.95
View factor	1

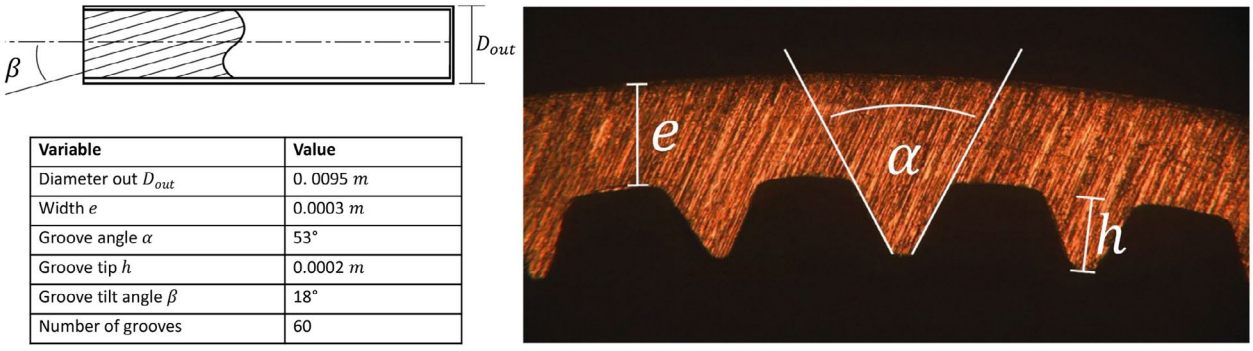

Variable	Value
Diameter out D_{out}	0. 0095 m
Width e	0.0003 m
Groove angle α	53°
Groove tip h	0.0002 m
Groove tilt angle β	18°
Number of grooves	60

Fig. 1. Geometric characteristics of the grooved tube.

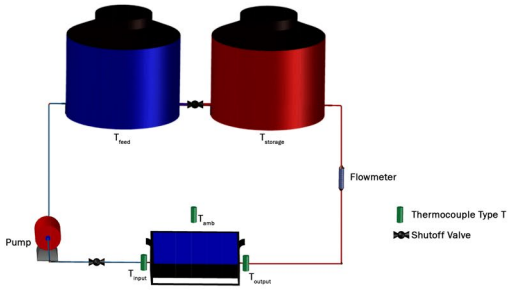

Fig. 2. Schematic diagram of the PTC experimental system.

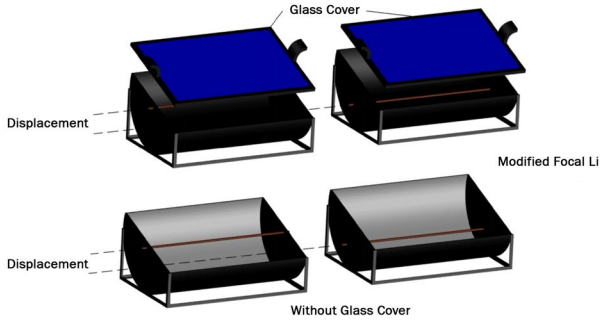

Fig. 3. Arrangement configurations of the PTC experimental system.

to avoid optical losses, (c) with glass lid and receiver tube located in a second focal line, and (d) without glass lid and receiver tube situated in second focal line. The experimental tests were carried out at different volumetric flows: 0.7, 1, 2, 3, 4, and 5 LPM using water as a working fluid. A total of 1,155 samples were recorded during October and November from 10:00 to 18:00 h, with intervals of 5 min between measurements. Table 2 shows the operating ranges to which the PTC system was subjected.

Irradiance data were collected using a pyranometer located at a Meteorological Station [21]. The calculation of the day of the year was made based on Table 3, where i is the day of the month calendar, and the time of day was established in minutes.

Table 2
Operating conditions of the PTC system

Experimental variables	Working range
Day	287–318
Flow, LPM	0.7–5
Configuration	1–4
Hour, min	595–1,085
Irradiance, W/m^2	2–1,043
T_{input}, °C	20.01–38.11
T_{env}, °C	19.27–39.02
T_{feed}, °C	18.18–28.95
$T_{storage}$, °C	18.75–30.72
T_{output}, °C	20.02–41.99

3. Development of the neural network model

ANNs are computational algorithms inspired by the learning process of the human brain. Like a biological neural network, ANNs are formed by parallel processing units called neurons, which generate and send information signals to produce a specific response output [22]. In different fields of knowledge, it has been defined as an efficiently mathematical modeling tool of linear and nonlinear multivariate regression problems [23].

From a certain amount of information, the ANNs have the capacity to discern the relationship between the variables of a process and recognize behavior patterns when they are challenging to describe them mathematically [24]. They are useful when the data comes from nonlinear processes, which inherently have noise; specifically, the data coming from renewable energy systems since it is difficult to identify a precise mathematical function when some parameters vary by time and environmental factors [13].

To develop an ANN model requires three fundamental tasks. The first task is the creation of a working database provided by the measurement of operation variables through instrumentation equipment. It is essential to mention that the variables considered for the model should preferably be representative of the phenomenon to reduce the size of the network and avoid redundancy in training data. Besides, its analysis with statistical processes is recommended [25].

The second task is to obtain an adequate network configuration to reach an accurate prediction. In this step, the size and normalization of the data set, the number of hidden neurons, the training algorithm, and the activation function are essential parameters to be considered. So that later, in the third task, the correlation between obtained and experimental variables is established.

Three layers mainly characterize the neural network model configuration. The first layer, known as the input layer, contains the variables that will be considered as input neurons in the model. A normalization or standardization process should be applied to input data to adjust them on the same scale. This process allows comparing its proportions instead of their magnitudes and offers a considerable decrease in the calculation time [26].

Table 3
Calculation of the day of the year

Month	Day of the year
January	i
February	31+i
March	59+i
April	90+i
May	120+i
June	151+i
July	181+i
August	212+i
September	243+i
October	273+i
November	304+i
December	334+i

The normalization of the database prevents mathematical saturation since sigmoid transfer functions tend to become saturated when presenting values higher than +3 or less than –3. Having a high number of values on the input variables, the amount assigned to the weights must be minimal what would make the training very slow [27]. The normalization interval of the input variables must be related to the activation function that is decided to be used. Usually, it is done in intervals from –1 to 1, for which there are different equations in the literature.

The second layer is the hidden layer, where are one or more processing units called hidden neurons. The accurate prediction of the ANN model is determined by the number of these units associated with their activation function. Lastly, in the output layer, through a matrix of weights and bias, be interconnected all the neurons of the model for generating the variable(s) to predict.

To each hidden neuron is required the network input term n_j that consists of a group of connection links called synapses; where each of these has an adjustable connection value, called synaptic weight Wi, which can be positive if the neuron increases the activation state of the adjacent or negative neuron if it inhibits it. The weight product and its respective input P are summed for each neuron by adding an offset value b known as bias [28], as shown in the following expression:

$$n_j = \mathrm{Wi}_{(j,1)} \cdot P_{(1)} + \mathrm{Wi}_{(j,2)} \cdot P_{(2)} + \ldots + \mathrm{Wi}_{(j,r)} \cdot P_{(r)} + b_{(1,j)} \tag{1}$$

where Wi are the coefficients of the connection weights between the input layer and the hidden layer, P are the input variables, j is the number of neurons in the hidden layer, r is the number of input neurons, and b is the bias corresponding to each neuron in the hidden layer.

An activation or transfer function is applied to n_j in order to determine the magnitude of response of each hidden neuron. There are a different transfer or activation functions as hard-limit, linear, logarithmic sigmoid, hyperbolic tangent sigmoid, Gaussian, among others. The most prominent functions for the hidden layer are the tangential-sigmoidal function (TANSIG, τ) and the logarithmic-sigmoidal (LOGSIG, δ). Their equations are shown in Table 4. Normally, a linear transfer function (PURELIN, λ) is used for the output layer [29]. An ANN model is generally represented according to the activation function selected.

For the learning process, the most common architecture used has been multilayer perceptron trained with the Levenberg–Marquardt backpropagation training algorithm in a feed-forward multilayer network [30], which have been recommended for heat exchanger analysis [31] and the performance of a solar collector [32].

To validate the accuracy and the adaptability of the model proposed, statistical tests are performed to analyze the experimental data and simulated data obtained. The test parameters that commonly used are the root mean square error RMSE, mean absolute percent error MAPE, and the coefficient of determination R^2 [17]. The optimal model is the one with the highest R^2, and the lowest MAPE, and RMSE.

$$R^2 = 1 - \frac{\sum_{i=1}^{n}\left(x_{\exp(i)} - x_{\mathrm{sim}(i)}\right)^2}{\sum_{i=1}^{n}\left(x_{\exp(i)} - \bar{x}_{\exp}\right)^2} \tag{2}$$

$$\mathrm{MAPE} = \frac{\sum_{i=1}^{n}\left|\frac{x_{\exp(i)} - x_{\mathrm{sim}(i)}}{x_{\exp(i)}}\right|}{n} \times 100(\%) \tag{3}$$

$$\mathrm{RMSE} = \sqrt{\frac{\sum_{i=1}^{n}\left(x_{\mathrm{sim}(i)} - x_{\exp(i)}\right)^2}{n}} \tag{4}$$

Significance tests are applied to the relation of experimental and simulated databases to corroborate the fit of the model. The F-test or Fisher test and Student's t-test are the significance tests more used to analyze the null hypothesis H_0 or the alternative hypothesis H_1 [33]. The H_0 establishes: if

Table 4
Equations of the TANSIG and LOGSIG transfer functions

Activation function	TANSIG	LOGSIG
Mathematical form	$\tau = \frac{e^{n_j} - e^{-n_j}}{e^{n_j} + e^{-n_j}} = \frac{2}{1+e^{-2n_j}} - 1$	$\delta = \frac{1}{1+e^{-n_j}}$
General equation	$\tau(n_j) = \frac{2}{1+e^{\left[-2\sum_{j=1}^{1}\left(\mathrm{Wi}_{(j,r)} \cdot P_{(r)} + b_{(1,j)}\right)\right]}} - 1$	$\delta(n_j) = \frac{1}{1+e^{-\left[\sum_{j=1}^{1}\left(\mathrm{Wi}_{(j,r)} \cdot P_{(r)} + b_{(1,j)}\right)\right]}}$
Simplified output equation	$\mathrm{Output} = \lambda\left(\mathrm{Wo}_{(K,J)} \cdot \tau(n_j) + b_{(2,K)}\right)$	$\mathrm{Output} = \delta\left(\mathrm{Wo}_{(K,J)} \cdot \delta(n_j) + b_{(2,K)}\right)$
General output equation	$\mathrm{Output} = \sum_{k=1}^{K}\left\{\mathrm{Wo}_{(K,J)}\left[\frac{2}{1+e^{\left[-2\sum_{j=1}^{1}\left(\mathrm{Wi}_{(J,R)} \cdot P_{(R)} + b_{(1,J)}\right)\right]}} - 1\right]\right\} + b_{(2,K)}$	$\mathrm{Output} = \sum_{k=1}^{K}\left\{\mathrm{Wo}_{(K,J)}\left[\frac{1}{1+e^{-\left[\sum_{j=1}^{1}\left(\mathrm{Wi}_{(J,R)} \cdot P_{(R)} + b_{(1,J)}\right)\right]}}\right]\right\} + b_{(2,K)}$

the two databases have the same variance or similar variance (*F*-test), or if the mean of two databases are equal or comes from the same population (*t*-test). Likewise, the H_1 determines that the variance or mean of databases is different. The critic value computed must be less to critic value from the statistical tables to accept H_0. For calculate *F*-test and *t*-test, the following equations are used:

$$S = \sqrt{\frac{\sum_{i=1}^{n_{exp}}\left(x_{exp(i)} - \bar{x}_{exp(i)}\right)^2 + \sum_{i=1}^{n_{sim}}\left(x_{sim(i)} - \bar{x}_{sim(i)}\right)^2}{\left(n_{exp} + n_{sim} - 2\right)}} \tag{5}$$

$$F = \frac{S_{exp}^2}{S_{sim}^2} \tag{6}$$

$$t = \frac{\left|\overline{x_{exp}} - \overline{x_{sim}}\right|}{S\left(\sqrt{\left(\frac{1}{n_{exp}} + \frac{1}{n_{sim}}\right)}\right)} \tag{7}$$

The parameter *S* is the standard deviation combined. For the *F*-test, the calculated *F* must always be ≥1. In case it is lower, it must be recalculated with the inverted terms. The numerator must always be higher or equal to the denominator. When the *F*-test is approved, the student's *t*-test is carried out. Otherwise, it is not applied, and the model must be rejected [34].

To validate the relationship between the simulated data with the ANN model and the experimental data, linearity tests are performed. It is known in advance that the linear regression analysis is used to obtain a relationship between two variables (one dependent and the other independent) and thus estimate the coefficients of the slope and the intercept, which determines the equation of the line. Statistically, the slope must be equal to 1 and the intercept equal to 0 [33].

The slope-intercept linearity test also called the standard deviation of the linear regression or standard error, establishes the confidence limits of the slope and intercept. These limits or intervals should ideally be one and zero for the slope and the intercept, respectively [35]. By the following equations, the errors on the linear regression coefficients are estimated:

$$S_b = \sqrt{\frac{\sum_{i=1}^{n}\left(x_{sim(i)} - \hat{x}_{sim(i)}\right)^2}{(n-2)\sum_{i=1}^{n}\left(x_{exp(i)} - \bar{x}_{exp(i)}\right)^2}} \tag{8}$$

and

$$S_a = \sqrt{\frac{\sum_{i=1}^{n}\left(x_{sim(i)} - \hat{x}_{sim(i)}\right)^2 \sum_{i=1}^{n} x_{exp(i)}^2}{n(n-2)\sum_{i=1}^{n}\left(x_{exp(i)} - \bar{x}_{exp}\right)^2}} \tag{9}$$

where $x_{sim(i)}$ is the simulated value and $\bar{x}_{sim(i)}$ the value of x_{sim} calculated by linear regression for the same value at $x_{sim(i)}$ ($\hat{x}_{sim} = a + b\bar{x}_{exp(i)}$) [36]. The expression $x_{sim(i)} - \hat{x}_{sim(i)}$ is called residual, which comes from the original data with respect to the regression line.

At this point, it is important to remember that the slope *b* is given by:

$$b = \frac{\sum_{i=1}^{n}\left\{\left(x_{exp(i)} - \bar{x}_{exp}\right)\left(x_{sim(i)} - \bar{x}_{sim}\right)\right\}}{\sum_{i=1}^{n}\left(x_{exp(i)} - \bar{x}_{exp}\right)^2} \tag{10}$$

The intercept *a* for:

$$a = \bar{x}_{sim} - b\bar{x}_{exp} \tag{11}$$

where $\bar{x}_{exp}$ and $\bar{x}_{sim(i)}$ are the mean of the experimental and simulated data, respectively.

Therefore, the confidence intervals or limits of the slope and the intercept will be defined as:

$$\text{to slope}\left\{b - \left(t_{(n-2)}s_b\right)\right\} < \mu_b < \left\{b + \left(t_{(n-2)}s_b\right)\right\} \tag{12}$$

$$\text{to intercept}\left\{a - \left(t_{(n-2)}s_a\right)\right\} < \mu_a < \left\{a + \left(t_{(n-2)}s_a\right)\right\} \tag{13}$$

where $t_{(n-2)}$ is the critical value *t* of Student that comes from statistic tables, at a certain level of confidence or significance of 95% or 99% (recommended) with *n*–2 degrees of freedom. For *n* bivariate data, the degrees of freedom will be reduced by two because of at least two data or points are required to draw a straight line of regression [33]. However, an adjustment is necessary when the data exceeds one thousand samples; this adjustment is mainly for 98% and 99% levels (for both sides). The expressions are as follows [34]:

Less or equal than 1,000 data and a 98% confidence level:

$$\begin{aligned}\left(t_{98ts}^{cv}\right)_{int} = {} & \left(4.94002103 \pm 0.00012294\right) - \left(4.5022554 \pm 0.0018112\right)\times\left(\ln\left(\ln\left(n\right)\right)\right) + \left(2.785764 \pm 0.008079\right)\times\left(\ln\left(\ln\left(n\right)\right)\right)^2 - \\ & \left(0.485943 \pm 0.016415\right)\times\left(\ln\left(\ln\left(n\right)\right)\right)^3 - \left(0.3051890 \pm 0.017282\right)\times\left(\ln\left(\ln\left(n\right)\right)\right)^4 + \left(0.216257 \pm 0.009455\right)\times \\ & \left(\ln\left(\ln\left(n\right)\right)\right)^5 - \left(0.0506048 \pm 0.0022587\right)\times\left(\ln\ln\left(\ln\ln\left(n\right)\right)\right)^6 + \left(0.00132479 \pm 0.000062583\right)\times\left(\ln\left(\ln\left(n\right)\right)\right)^8\end{aligned} \tag{14}$$

To more than 1,000 data and a 98% confidence level:

$$\left(t_{98ts}^{cv}\right)_{ext} = \left(4.94237021 \pm 0.00014897\right) - \left(4.5412456 \pm 00.0007948\right) \times \left(\ln\left(\ln\left(n\right)\right)\right) + \left(2.9690047 \pm 0.0013459\right) \times \left(\ln\left(\ln\left(n\right)\right)\right)^2 - \left(0.8658555 \pm 0.0008820\right) \times \left(\ln\left(\ln\left(n\right)\right)\right)^3 + \left(0.09497881 \pm 0.00019659\right) \times \left(\ln\left(\ln\left(n\right)\right)\right)^4 \quad (15)$$

Less or equal than 1,000 data and a 99% confidence level:

$$\left(t_{99ts}^{cv}\right)_{int} = \left(6.48557253 \pm 0.00017748\right) - \left(7.3462223 \pm 0.0026146\right) \times \left(\ln\left(\ln\left(n\right)\right)\right) + \left(5.418770 \pm 0.011663\right) \times \left(\ln\left(\ln\left(n\right)\right)\right)^2 - 1.721741 \pm 0.023697) \times \left(\ln\left(\ln\left(n\right)\right)\right)^3 - \left(0.0930165 \pm 0.024949\right) \times \left(\ln\left(\ln\left(n\right)\right)\right)^4 + \left(0.274850 \pm 0.013649\right) \times \left(\ln\left(\ln\left(n\right)\right)\right)^5 - \left(0.0779639 \pm 0.0032607\right) \times \left(\ln\left(\ln\left(n\right)\right)\right)^6 + \left(0.00221624 \pm 0.00009035\right) \times \left(\ln\left(\ln\left(n\right)\right)\right)^8 \quad (16)$$

and, more than 1,000 data and a 99% confidence level:

$$\left(t_{99ts}^{cv}\right)_{ext} = \left(2.94230900 \pm 0.00003147\right) - \left(1.1213450 \pm 0.00018085\right) \times \left(\ln\left(\ln\left(\ln\left(n\right)\right)\right)\right) + \left(0.78201429 \pm 0.00031542\right) \times \left(\ln\left(\ln\left(\ln\left(n\right)\right)\right)\right)^2 + \left(0.3639632 \pm 0.0009774\right) \times \left(\ln\left(\ln\left(\ln\left(n\right)\right)\right)\right)^3 - \left(0.20510287 \pm 0.00048796\right) \times \left(\ln\left(\ln\left(\ln\left(n\right)\right)\right)\right)^4 - \left(0.1945693 \pm 0012343\right) \times \left(\ln\left(\ln\left(\ln\left(n\right)\right)\right)\right)^5 - \left(0.04167330 \pm 0.00042639\right) \times \left(\ln\left(\ln\left(\ln\left(n\right)\right)\right)\right)^6 \quad (17)$$

Finally, the Garson equation [37] was used to determine the importance of the input variables within the network; this equation is based on the partition of the weight connections.

$$I_P = \frac{\sum_{j=1}^{J}\left(\left(\frac{\left|W_{(P,J)}\right|}{\sum_{r=1}^{R}\left|W_{(R,J)}\right|}\right) \times \left|W_{(J,K)}\right|\right)}{\sum_{r=1}^{R}\left\{\sum_{j=1}^{J}\left(\left(\frac{\left|W_{(R,J)}\right|}{\sum_{r=1}^{R}\left|W_{(R,J)}\right|}\right) \times \left|W_{(J,K)}\right|\right)\right\}} \quad (18)$$

where I_P is the relative importance of the input variable P over the output variable.

4. Neural network model

For a neural network model to learn to calculate the output variable with high precision is necessary to establish the topology or architecture accurately. The normalization of the input data, the number of neurons in the hidden layer, and the degree of connectivity obtained through the transfer function are essential parameters to be determined.

Like a biological neuron, the artificial neuron calculates its degree of connectivity from the activation function. In simple terms, a transfer or activation function of a neuron represents the potential rate at which a neuron is activated or not. Its primary purpose is to relate an output response to the input signals varying in the range of –1 to 1, depending on the selected transfer function. Therefore, the normalization interval of the input variables must be related to the activation function that is decided to be used.

As mentioned earlier, the normalization process prevents mathematical saturation when transfer functions are used. When the values of the input variables are very high, the weight values obtained will be very small. Therefore, the descending gradient in the process will be short, which leads to prolonged training [27]. This behavior is independent of what the bias has, since these only act as compensation or counterweight value for the network.

In the literature, various equations of normalizations have been applied for some transfer functions. In a paper reported by Hernández and Colorado [38], different transfer functions were evaluated varying intervals of normalization in an absorption heat transformer with energy recycling. It was determined that the TANSIG function with a normalization range [0,1] showed better results compared to others. However, it exists some uncertainty choosing the appropriate transfer function and normalization process, as well as the optimal number of neurons in the hidden layer. Therefore, in this work, in order to discern the best topology, it was required to make an analysis of the transfer functions at different normalization intervals and find the best model capable of estimating of PTC outlet temperature.

A first network model was developed that was used as a base model from 1,155 concordant experimental data. Nine variables were selected, which was being considered significant for our PTC system. The input variables were the input temperature of the fluid, ambient temperature, irradiance, hour, day, configuration, volumetric flow, feeding temperature, and storage temperature.

This model was trained with 50% of the data, validated with 25%, and tested with the remaining 25%. The percentages above are those recommended for randomly dividing

the original sample into three sub-samples and thereby generating results with statistically significant precision [39]. This type of stratified sampling ensures that each element of the population has the same probability of being selected to integrate each one of the subsamples. When proposing an ANN model based on a single data sample, it could present significant errors. A multilayer feedforward backpropagation architecture was used with nine input neurons in a normalization interval from –1 to 1, the specified range for the TANSIG function. The general form of the normalization equation is represented as follows:

$$x_n = \left(y_{\max} - y_{\min}\right) \times \left(\frac{x_i - x_{\min}}{x_{\max} - x_{\min}}\right) + y_{\min} \tag{19}$$

where $y_{\max}$ and $y_{\min}$ are the limit values of the normalization interval. For this model, the values of $y_{\max}$ and $y_{\min}$ were 1 and –1, respectively. Once the neuronal model was obtained, the comparison between the simulated data and the experimental data was performed using the R^2, MAPE, and RMSE statistical tests described above.

Table 5 shows the comparison of the statistical analysis to determine the number of neurons in the hidden layer. It is observed that both the RMSE and the MAPE show a slight decrease for the five and six neuron configurations. Therefore, continuing to increase the number of neurons in the hidden layer would reduce in minimum values the error and increase the number of coefficients in the output equation, which generates over-fitting. Fig. 4 shows the architecture employed in the neural model of T_{output} with six hidden neurons.

Additionally, the *F*-test and *t*-test significance tests were performed on the ANN model. A significance level of 0.01 (99% confidence) was selected to indicate an acceptable error of 1%, and the *p*-value was determined to establish the minimum level of significance to accept the model. Table 6 shows the values obtained from the Fisher and *t*-student *F*-tests and the *p*-value.

The slope-intercept test was performed to verify that the simulated data is within the range defined by the limits of the target and not outside it. The values of the

Table 5
Statistical analysis of the neurons number in the hidden layer for base ANN model

Number of neurons	R^2	RMSE	MAPE
1	0.970366963	0.411245901	0.022058509
2	0.977060605	0.361024753	0.028778328
3	0.984686936	0.294146581	0.040628118
4	0.988624436	0.253367799	0.019870286
5	0.995204523	0.164814324	0.009307217
6	0.996191094	0.147062448	0.007954328

Table 6
Significance tests (Fisher test, *t*-student test, and *P*-value)

	Fisher test	*t*-student test
Calculated value (Eqs. (6) and (7))	1.00583512	0.44966639
Critic value (from tables)	1.14688062	2.32958361
If computed value < critic value	Yes	Yes
P-value		0.92129576

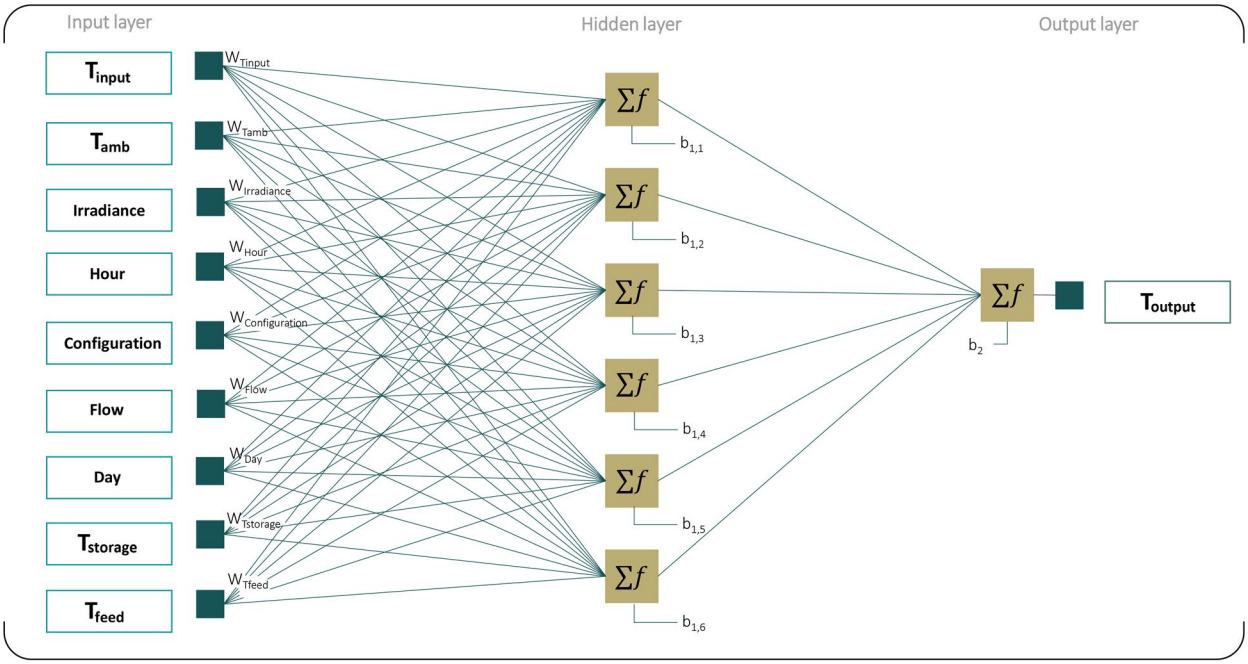

Fig. 4. Neural model architecture of the PTC with nine inputs.

pending-intercept test are presented in Fig. 5, where the base model is ratified. Where the lower intercept must be less than zero, and the upper intercept must be greater than zero. Similarly, the lower and upper slope must be less than and greater than 1, respectively. When averaging the resulting values should be close to zero for the intercept and one for the slope.

Fig. 6 shows the simulation of the outlet temperature of the collector using the base model on October 20 and 27, where it is observed that the model fits the experimental data satisfactorily despite the noise in the measurements.

To determine the influence of the normalization process influenced transfer functions, five areas of interest were identified for the use of TANSIG and LOGSIG functions, which are the most widely employed. The training process for the comparison is shown in Fig. 7, and the normalization intervals analyzed are shown in Fig. 8.

Consequently, ten models were developed for the analysis of the proposed normalization intervals using the same architecture as the base model. In the same way, the statistical parameters were calculated in order to validate them, and the results are shown in Table 7 for each normalization interval. As can be seen, similar values of R^2, RMSE, and MAPE were obtained in comparison with the base model, and even some reached a better value, as was the case with normalization in the interval [0.1,0.9] for TANSIG or with [0.1,0.5] for LOGSIG.

Fisher and Student *t*-tests were successfully applied and approved for most models. The results of significance tests are shown in Table 8. With respect to the slope-intercept test, the TANSIG model with normalization [–0.5, 0.5] and the LOGSIG model with [0.5,0.9] did not pass the test with any confidence level; despite having chosen 99%, 98%, and 95% of confidence. The results of the slope-intercept test for all models are exhibited in Table 9.

As shown in Figs. 9 and 10, the comparison between all data simulated by the models proposed with the experimental data reveals that, for this case, the slope-intercept test does not have importance in obtaining an accurate predictive model of our system. However, as can be observed, the model that got the smallest error, approved all tests and, showed the best fit was the TANSIG model with normalization [0.1,0.9].

The normalization process also has been suggesting used in the output variables. Hence, the normalization of the output variable was implemented in the models previously proposed. This procedure is not often used due to the PURELIN linear transfer function is the most handled in the output layer. The PURELIN transfer function has no restrictions; that is, it can take values from $-\infty$ to $+\infty$. However, the normalization of the output variables could improve model predictions but is necessary to denormalize output data for being used. The validation of these models was carried

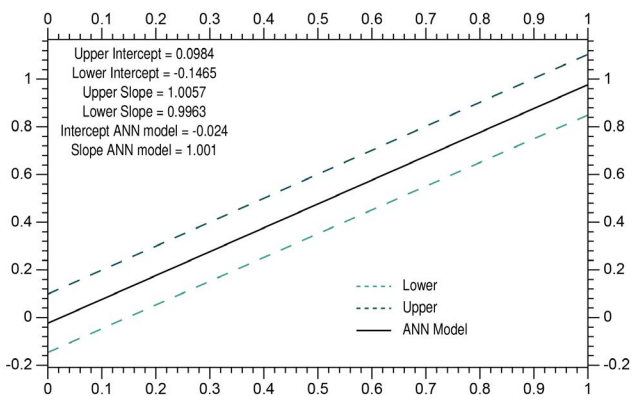

Fig. 5. Linearity test of the base ANN model.

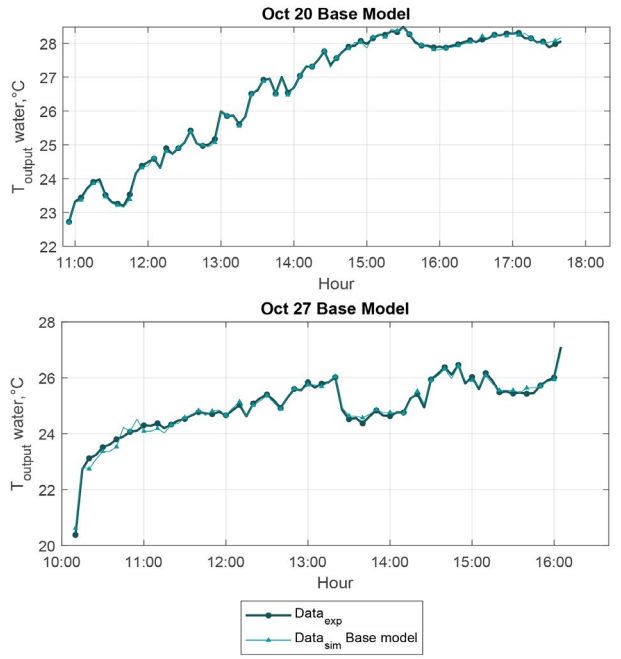

Fig. 6. Comparison between experimental and simulated data by base ANN model.

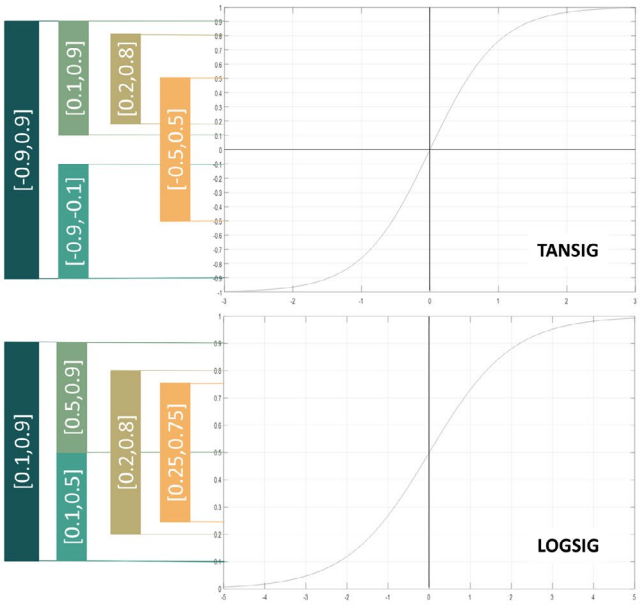

Fig. 7. Normalization intervals for TANSIG and LOGSIG transfer functions.

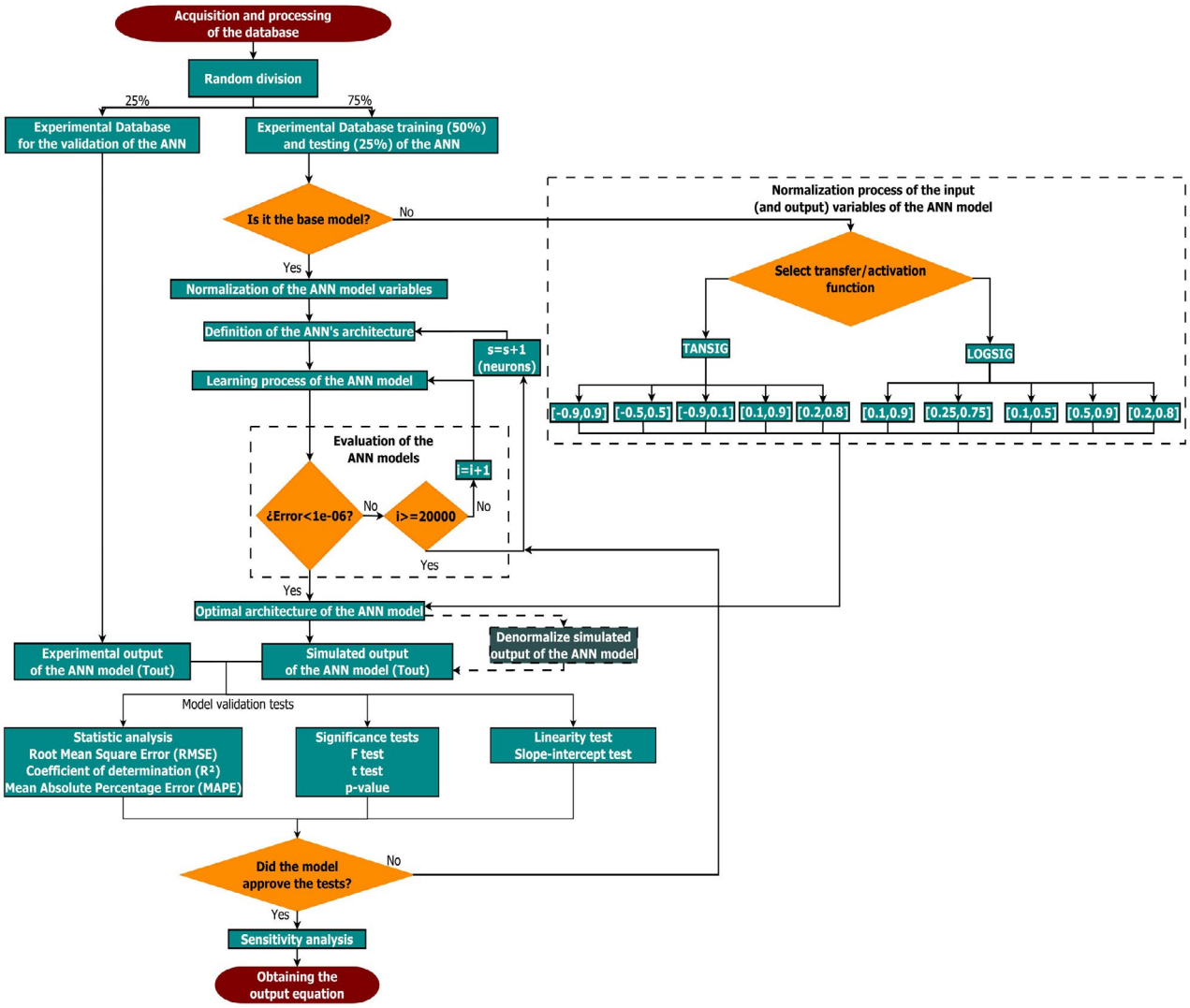

Fig. 8. Numerical method for the ANN learning process.

out through statistical tests, and Table 10 shows the results obtained.

Evidently, the models with normalized output acquired similar results who get with the base model. Note that when the modeling with ANN used normalized output, the RMSE is very smallest. The model with normalization in the interval of [–0.9, 0.9] for TANSIG was discarded because it did not approve the significance tests, as exhibits in Table 11. Figs. 11 and 12 show a comparison between the data simulated by models with normalized output and experimental data; as can be seen, the rejected model presented more dispersion compared to the other models.

Contrary to what happens with models with non-normalized outputs, Table 12 shows that there were very few models that approved the slope-intercept test. Only the models TANSIG of [–0.5,0.5], LOGSIG of [0.5,0.9], LOGSIG of [0.2,0.8], and LOGSIG [0.25,0.75] approved the test. It is essential to highlight that when the model ANN uses the TANSIG transfer function, avoiding the output normalization, normalizations that consider negative intervals had worse performance.

As it may be noted, all models fit right but have been considered that the best model was the TANSIG model with normalization in an interval of [0.1,0.9], which was that got the smallest error by statistical tests, approved the significance tests, and submitted minor dispersion. It has the highest R^2, the smallest MAPE, and the minimal RMSE without considering the models with standardized output (R^2 = 0.997405465, RMSE = 0.121237247, and MAPE = 5.9341 × 10^{-5}). In fact, this normalization interval has been wide reported by some authors [18,26,29,38,40]. Fig. 13 shows the accuracy check of the best ANN model.

Once the model was validated, the equation was obtained to determine the outlet temperature of the collector. The final architecture of the model was of nine neurons in the input layer, six neurons in the hidden layer, and one in the output layer. As it has a TANSIG transfer function in the hidden layer and PURELIN transfer function in the output layer, the equation is described as follows:

Table 7
Statistical analysis of ANN models with normalization intervals proposed for TANSIG and LOGSIG

Statistical analysis	TANSIG					LOGSIG				
	[–0.9,0.9]	[–0.9,–0.1]	[0.1,0.9]	[0.2,0.8]	[–0.5,0.5]	[0.1,0.9	[0.1,0.5]	[0.5,0.9]	[0.2,0.8]	[0.25,0.75]
R^2	0.996221316	0.995597257	0.997405465	0.9964935	0.99624876	0.99624533	0.99671914	0.99618892	0.9962321	0.99610716
RMSE	0.146385282	0.157763969	0.121237247	0.14086828	0.145702771	0.14636318	0.1361285	0.14724789	0.14737937	0.14836108
MAPE	0.04043158	0.01724422	5.9341E–05	0.00145046	0.02207994	0.008941	0.00252443	0.0162055	0.02743816	0.00199189

Table 8
Significance tests (Fisher test, *t*-student test, and *P*-value) for the comparison of normalization intervals TANSIG and LOGSIG

Function	Intervals	*F*-calculated (Eq. (6))	*t*-student calculated (Eq. (7))	If calculated value < critic value [*F*-test, *t*-test]	*P*-value (α = 0.01)
	[–0.9, 0.9]	1.00084628	2.26123776	[Yes, Not]	0.02393009
	[–0.9,–0.1]	1.00043807	1.05231189	[Yes, Yes]	0.29287677
TANSIG	[0.1,0.9]	1.00383619	0.01545336	[Yes, Yes]	0.98767317
	[0.2,0.8]	1.00289051	0.05134121	[Yes, Yes]	0.95906251
	[–0.5, 0.5]	1.00711859	1.59383554	[Yes, Yes]	0.11124671
	[0.1,0.9]	1.00896994	0.65140059	[Yes, Yes]	0.51491762
	[0.1,0.5]	1.00028414	0.06101505	[Yes, Yes]	0.95135779
LOGSIG	[0.5,0.9]	1.01500877	0.54525118	[Yes, Yes]	0.58568614
	[0.2,0.8]	1.01312795	1.76914282	[Yes, Yes]	0.07713413
	[0.25,0.75]	1.00173861	0.05659824	[Yes, Yes]	0.95487504
Critic value (from tables)		1.14688062	2.32958361	Significance lvl. 99% (α = 0.01)	p–value > α

Table 9
Values of linearity test (slope-intercept test)

Interval	TANSIG					LOGSIG				
	[–0.9,0.9]	[–0.9,–0.1]	[0.1,0.9]	[0.2,0.8]	[–0.5,0.5]	[0.1,0.9	[0.1,0.5]	[0.5,0.9]	[0.2,0.8]	[0.25,0.75]
Upper intercept	0.191250	0.189170	0.08505	0.12565772	0.25423	0.057478	0.15247	0.36510	0.00948925	0.15183
Intercept	0.069691	0.057926	–0.015916	0.00833601	0.13348	–0.064292	0.039133	0.24387	–0.11274612	0.028288
Lower intercept	–0.051872	–0.073319	–0.11688	–0.1089857	0.01274	–0.18606	–0.074204	0.12264	–0.2349815	–0.095257
Upper slope	1.00240	1.00260	1.00450	1.00419279	0.99923	1.0073	1.0029	0.99534	1.0093389	1.00370
Slope	0.99769	0.997580	1.00060	0.99968671	0.99459	1.0026	0.9985	0.99069	1.00464409	0.99892
Lower slope	0.99302	0.992540	0.99674	0.99518063	0.98995	0.99791	0.99415	0.98603	0.99994929	0.99417

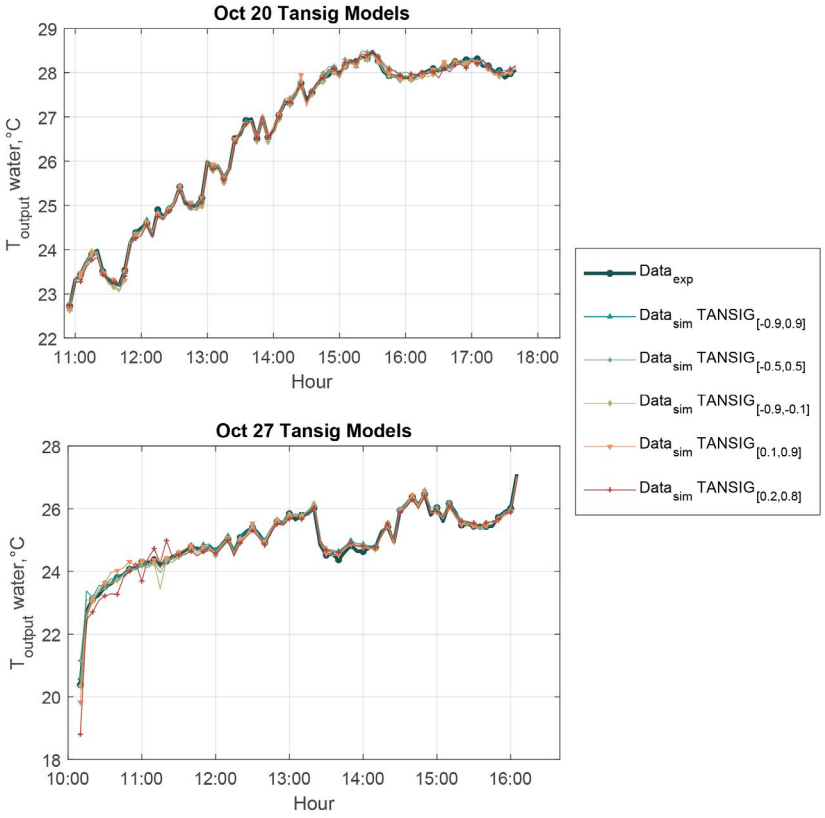

Fig. 9. Comparison between experimental and simulated data by TANSIG models.

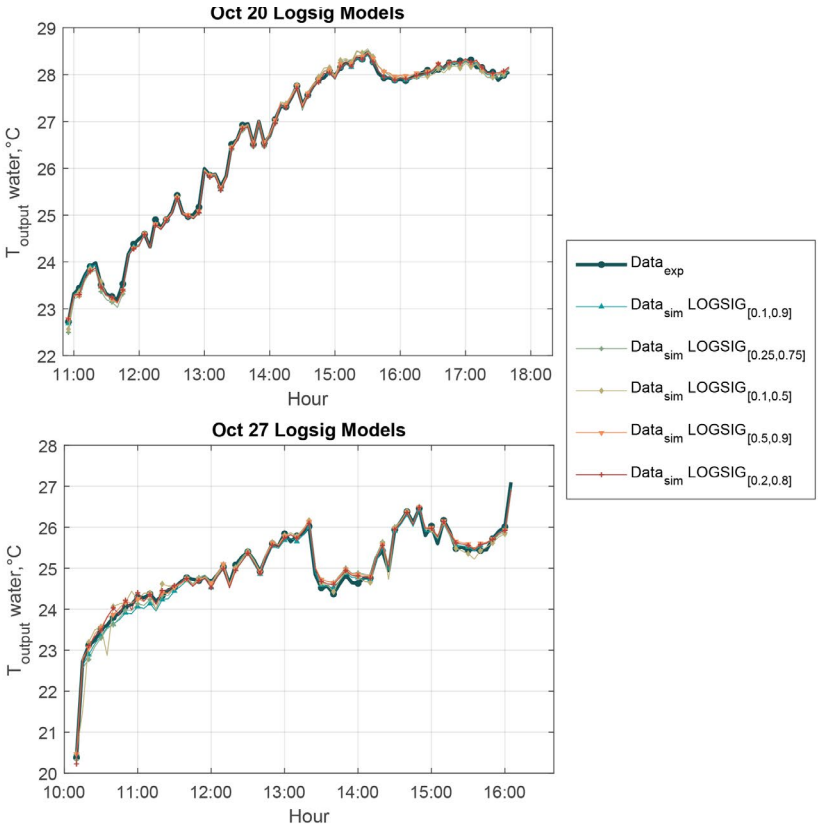

Fig. 10. Comparison between experimental and simulated data by LOGSIG models.

Table 10
Statistical analysis for the comparison at the same intervals TANSIG and LOGSIG with output normalized

Statistical analysis	TANSIG with normalized output					LOGSIG with normalized output				
	[–0.9,0.9]	[–0.9,–0.1]	[0.1,0.9]	[0.2,0.8]	[–0.5,0.5]	[0.1,0.9	[0.1,0.5]	[0.5,0.9]	[0.2,0.8]	[0.25,0.75]
R^2	0.996040	0.994909	0.996359	0.996011	0.996737	0.996021	0.996188	0.987329	0.997721	0.996639
RMSE	0.012302	0.006173	0.005227	0.004100	0.006179	0.005458	0.002689	0.004879	0.003111	0.003137
MAPE	0.476835	0.005938	0.038955	0.023999	0.321890	0.024467	0.054940	0.017070	0.019419	0.042913

Table 11
Significance tests (Fisher test, *t*–student test, and *P*-value) for the comparison at the same intervals TANSIG and LOGSIG with output normalized

Function	Intervals	*F*-calculated (Eq. (6))	*t*-student calculated (Eq. (7))	If calculated value < critic value [*F*-test, *t*-test]	*P*-value ($\alpha = 0.01$)
TANSIG with normalized output	[–0.9,0.9]	1.01015006	2.73958746	[Yes, Not]	0.00624644
	[–0.9,–0.1]	1.00806719	0.33356398	[Yes, Yes]	0.73876920
	[0.1,0.9]	1.00994680	0.08944406	[Yes, Yes]	0.92874453
	[0.2,0.8]	1.00000431	0.55675852	[Yes, Yes]	0.57780038
	[–0.5,0.5]	1.00095651	0.7103265	[Yes, Yes]	0.47764521
LOGSIG with normalized output	[0.1,0.9]	1.00715098	0.39782846	[Yes, Yes]	0.69083021
	[0.1,0.5]	1.01597356	2.29983889	[Yes, Yes]	0.02163516
	[0.5,0.9]	1.00132610	0.84987004	[Yes, Yes]	0.39557363
	[0.2,0.8]	1.00649484	0.78383054	[Yes, Yes]	0.43330040
	[0.25,0.75]	1.00274888	1.48134423	[Yes, Yes]	0.13878785
Critic value (from tables)		1.14688062	2.32958361	Significance lvl. 99% ($\alpha = 0.01$)	p-value > α

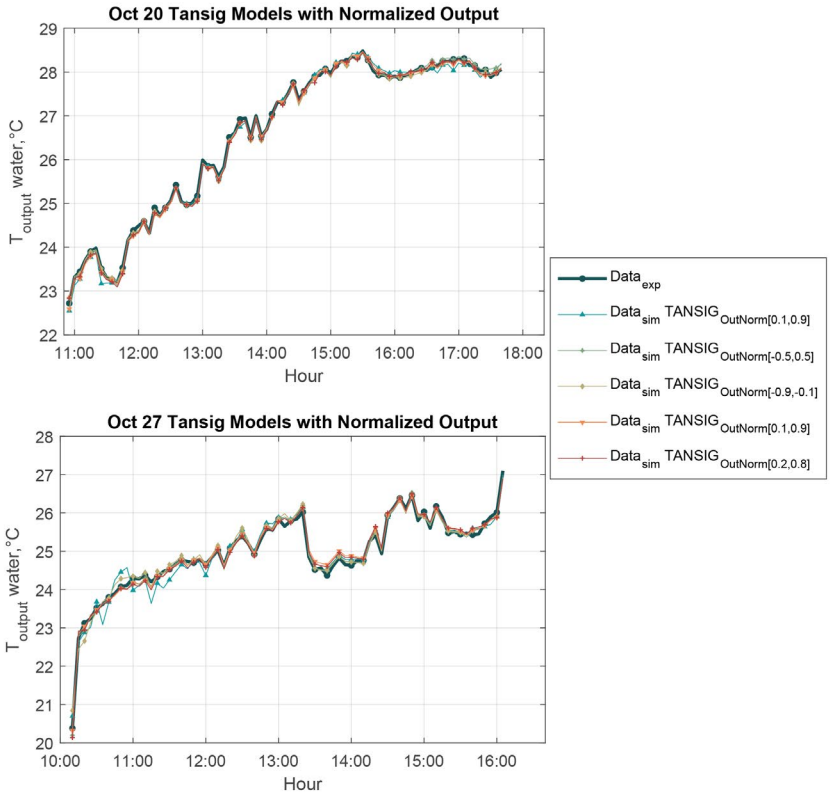

Fig. 11. Comparison between experimental and simulated data by TANSIG models with normalized output.

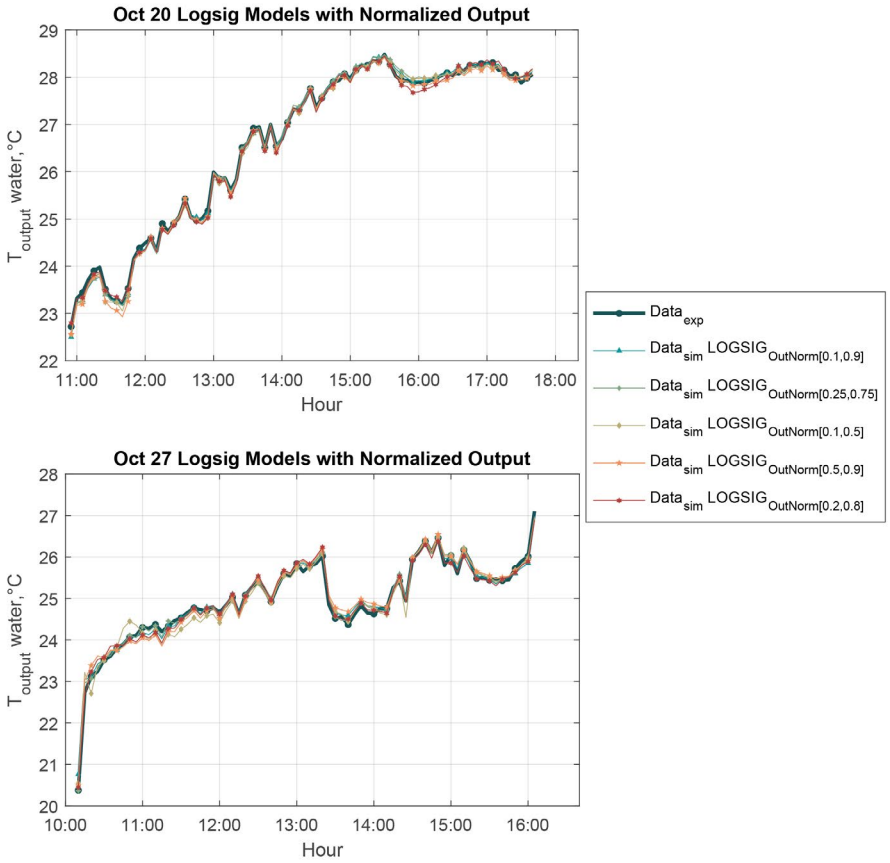

Fig. 12. Comparison between experimental and simulated data by LOGSIG models with normalized output.

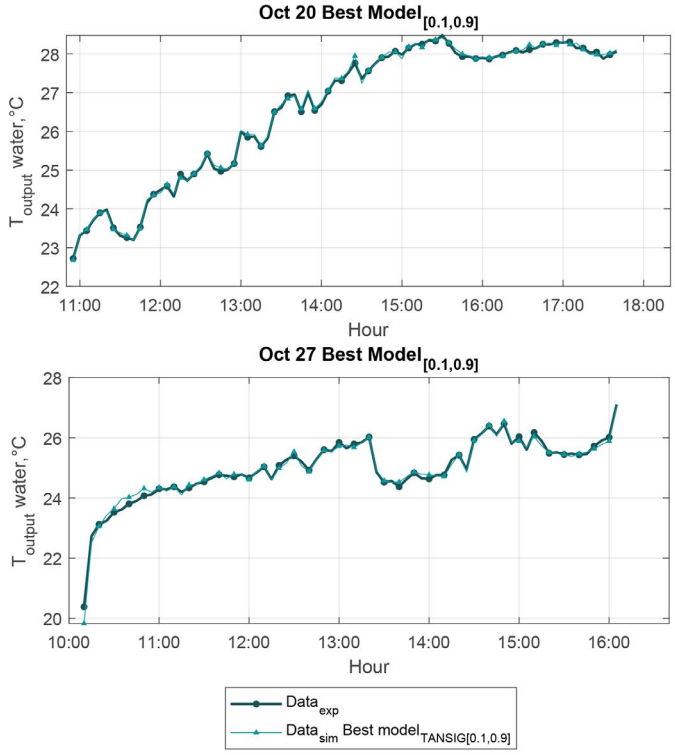

Fig. 13. Comparison between experimental and simulated data by best ANN model.

Table 12
Values of linearity test (slope-intercept test) for models with output normalized

Interval	TANSIG with normalized output					LOGSIG with normalized output				
	[–0.9,0.9]	[–0.9,–0.1]	[0.1,0.9]	[0.2,0.8]	[–0.5,0.5]	[0.1,0.9	[0.1,0.5]	[0.5,0.9]	[0.2,0.8]	[0.25,0.75]
Upper intercept	–0.00172	–0.00070	0.00363	0.00255	0.00075	0.00324	0.00284	0.00855	0.00065	0.00302
Intercept	–0.00390	–0.00442	0.00214	0.00079	–0.00036	0.00168	0.00185	0.00334	–0.00069	0.00131
Lower intercept	–0.00609	–0.00815	0.00065	–0.00097	–0.00147	0.00012	0.00086	–0.00187	–0.00202	–0.00040
Upper slope	0.99775	0.99885	0.99781	1.00280	1.00220	0.99924	0.99487	1.00290	1.00574	1.00130
Slope	0.99299	0.99345	0.99325	0.99800	0.99789	0.99446	0.99021	0.99430	1.00210	0.99695
Lower slope	0.98823	0.98805	0.98869	0.99320	0.99355	0.98968	0.98556	0.98574	0.99846	0.99255

Table 13
Weight and bias matrix of the best ANN model

Hidden Neuron	Wi (weights between input and hidden layers)							Wo (weights between hidden and output layers)		Bias	
	$R = 1$	$R = 2$	$R = 3$	$R = 4$	$R = 5$	$R = 6$	$R = 7$	$R = 8$	$R = 9$	$K = 1$	$b1$	$b2$
$J = 1$	–8.181033	2.322151	–19.318793	–2.233757	–1.30984	–0.444677	22.902622	–2.898441	–5.252849	2.468148	5.569662	
$J = 2$	1.010914	–0.711492	–10.320357	1.085409	0.535034	0.034638	–4.421108	–0.244466	0.937116	–3.205328	1.848974	
$J = 3$	17.250895	–15.348804	–0.046645	–32.671733	–41.374916	–25.451028	–1.450043	–3.126300	–7.311760	19.874896	27.534233	41.508457
$J = 4$	–0.247912	0.123911	0.066479	–0.008568	0.029014	–0.004724	–1.641045	0.290829	–0.029878	–19.918823	0.314045	
$J = 5$	3.372385	–5.309574	1.556534	–2.078800	–3.866334	3.895716	–5.421965	–1.765726	12.477538	–0.184265	–1.765766	
$J = 6$	–4.319783	1.765434	2.353920	1.963862	1.649682	0.875938	–20.490922	5.371282	2.670823	1.061698	1.913004	

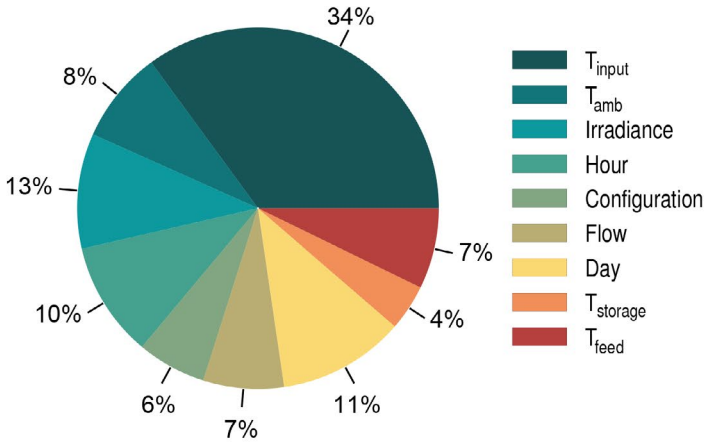

Fig. 14. Relative importance of the input variables in the best ANN model of PTC system.

$$T_{\text{output}} = \sum_{k=1}^{K}\left\{\text{Wo}_{(K,J)}\left[\frac{2}{1+e^{\left[-2\sum_{j=1}^{I}\left(\text{Wi}_{(J,R)}\cdot P_{(R)}+b_{(1,J)}\right)\right]}}-1\right]\right\}+b_{(2,K)} \tag{20}$$

Expressed in simple terms:

$$T_{\text{output}} = 2\left[\frac{\text{Wo}_{(1,1)}}{1+e^{(x_1)}}+\frac{\text{Wo}_{(1,2)}}{1+e^{(x_2)}}+\frac{\text{Wo}_{(1,3)}}{1+e^{(x_3)}}+\frac{\text{Wo}_{(1,4)}}{1+e^{(x_4)}}+\frac{\text{Wo}_{(1,5)}}{1+e^{(x_5)}}+\frac{\text{Wo}_{(1,6)}}{1+e^{(x_6)}}\right]-\left(\text{Wo}_{(1,1)}+\text{Wo}_{(1,2)}+\text{Wo}_{(1,3)}+\text{Wo}_{(1,4)}+\text{Wo}_{(1,5)}+\text{Wo}_{(1,6)}\right)+b_{(2,1)} \tag{21}$$

where

$$x_1 = -2\cdot\left(\text{Wi}_{(1,1)}\cdot P_1+\text{Wi}_{(1,2)}\cdot P_2+\text{Wi}_{(1,3)}\cdot P_3+\text{Wi}_{(1,4)}\cdot P_4+\text{Wi}_{(1,5)}\cdot P_5+\text{Wi}_{(1,6)}\cdot P_6+\text{Wi}_{(1,7)}\cdot P_7+\text{Wi}_{(1,8)}\cdot P_8+\text{Wi}_{(1,9)}\cdot P_9+\right)+b_{(1,1)} \tag{22}$$

:

$$x_6 = -2\cdot\left(\text{Wi}_{(6,1)}\cdot P_1+\text{Wi}_{(6,2)}\cdot P_2+\text{Wi}_{(6,3)}\cdot P_3+\text{Wi}_{(6,4)}\cdot P_4+\text{Wi}_{(6,5)}\cdot P_5+\text{Wi}_{(6,6)}\cdot P_6+\text{Wi}_{(6,7)}\cdot P_7+\text{Wi}_{(6,8)}\cdot P_8+\text{Wi}_{(6,9)}\cdot P_9+\right)+b_{(1,6)} \tag{23}$$

The values in Eq. (21) are replaced by weights and biases that are given in Table 13.
Replacing

$$T_{\text{output}} = 2\left[\frac{(2.468148)}{1+e^{(x_1)}}+\frac{(-3.205328)}{1+e^{(x_2)}}+\frac{(19.874896)}{1+e^{(x_3)}}+\frac{((-19.918823)}{1+e^{(x_4)}}+\frac{(-0.184265)}{1+e^{(x_5)}}+\frac{(1.061698)}{1+e^{(x_6)}}\right]-$$
$$\left[(2.468148)+(-3.205328)+(19.874896)+(-19.918823)+(-0.184265)+(1.061698)\right]+41.508457(21.b) \tag{24}$$

and

$$x_1 = -2\cdot\left[\begin{matrix}(-8.181033)\cdot P_1+(2.322151)\cdot P_2+(-19.318793)\cdot P_3+(-2.233757)\cdot P_4+(-1.30984)\cdot P_5+(-0.444677)\cdot\\ P_6+(22.902622)\cdot P_7+(-2.898441)\cdot P_8+(-5.252849)\cdot P_9\end{matrix}\right]+5.569662 \tag{25}$$

$$x_2 = -2\cdot\left[\begin{matrix}(1.010914)\cdot P_1+(-0.711492)\cdot P_2+(-10.320357)\cdot P_3+(1.085409)\cdot P_4+(0.535034)\cdot P_5+(0.034638)\cdot\\ P_6+(-4.421108)\cdot P_7+(-0.244466)\cdot P_8+(0.937116)\cdot P_9\end{matrix}\right]+1.848974 \tag{26}$$

$$x_3 = -2 \cdot \left[\begin{matrix} (17.250895) \cdot P_1 + (-15.348804) \cdot P_2 + (-0.046645) \cdot P_3 + (-32.671733) \cdot P_4 + (-41.374916) \cdot \\ P_5 + (-25.451028) \cdot P_6 + (-1.450043) \cdot P_7 + (-3.126300) \cdot P_8 + (-7.311760) \cdot P_9 \end{matrix} \right] + 27.534233 \quad (27)$$

$$x_4 = -2 \cdot \left[\begin{matrix} (-0.247912) \cdot P_1 + (0.123911) \cdot P_2 + (0.066479) \cdot P_3 + (-0.008568) \cdot P_4 + (0.029014) \cdot \\ P_5 + (-0.004724) \cdot P_6 + (-1.641045) \cdot P_7 + (0.290829) \cdot P_8 + (-0.029878) \cdot P_9 \end{matrix} \right] + 0.314045 \quad (28)$$

$$x_5 = -2 \cdot \left[\begin{matrix} (3.372385) \cdot P_1 + (-5.309574) \cdot P_2 + (1.556534) \cdot P_3 + (-2.078800) \cdot P_4 + (-3.866334) \cdot \\ P_5 + (3.895716) \cdot P_6 + (-5.421965) \cdot P_7 + (-1.765726) \cdot P_8 + (12.477538) \cdot P_9 \end{matrix} \right] + (-1.765766) \quad (29)$$

$$x_6 = -2 \cdot \left[\begin{matrix} (-4.319783) \cdot P_1 + (1.765434) \cdot P_2 + (2.353920) \cdot P_3 + (1.963862) \cdot P_4 + (1.649682) \cdot \\ P_5 + (0.875938) \cdot P_6 + (-20.490922) \cdot P_7 + (5.371282) \cdot P_8 + (2.670823) \cdot P_9 \end{matrix} \right] + 1.913004 \quad (30)$$

The Garson equation was used to realize the sensitivity analysis, which determine the importance of the input variables over the best model obtained. The sensitivity analysis depends exclusively on the weight given to each connection during training, that is, the values may vary from model to model with similar R^2, RMSE, and MAPE and the same architecture. The reason is that, during training, the connections are adjusted to be able to represent the experimental output variable. The results of the sensitivity analysis for the best model obtained are shown in Fig. 14.

As to be expected, with the result of the sensitivity analysis, it was determined that the variable with greater preponderance over the best model was the input temperature with 34%. It is known that the outlet temperature acquires values in relation to the inlet temperature of the fluid. The variables that follow in order of importance, such as irradiance and day of the year, reiterating how the season of the year represents an essential variable for the PTC system. The position of the Earth with respect to the Sun, significantly influences the amount of radiation absorbed by the PTC.

The next two variables, which are the time of day and the ambient temperature, clearly represent how the performance of the PTC system is closely related to the exposure time. On the other hand, the configuration shows a small impact over the model, which means that convection losses could be comparable to optical losses.

Even though the temperature of the feed tank and volumetric flow had a lower similar percentage than others, it could be variables to consider to increase the outlet temperature. Finally, the least important variable was the storage temperature, which can be depreciated because it represented directly by the inlet temperature due to there is a system in recirculation.

Other studies could be realized in the future to evaluate the relative importance of input variables over the model and determine numerically what variables are necessary to consider in the input layer.

5. Conclusions

A low-cost parabolic trough solar collector with an absorber grooved tube was installed as a cheap option for residential use. By experimental measurements of a water heating process, the PTC was modeled with ANNs in order to predict the output temperature.

To obtain a model with high precision, a training analysis using the TANSIG and LOGSIG transfer functions in the hidden layer was performed, considering different normalization intervals in both the input and output variables.

The best model was the one that obtained outstanding behavior according to the statistical, significance, and slope-intercept tests. This model used TANSIG as a transfer function with a normalization interval of [0.1,0.9]. A multilayer feedforward backpropagation architecture was proposed with a structure of nine neurons in the input layer, six neurons in the hidden layer, and one in the output layer. The input variables were the input temperature of the fluid, environment temperature, irradiance, hour, day, configuration, volumetric flow, feeding temperature, and storage temperature. The statistical results obtained were $R^2 = 0.9974$, RMSE = 0.12123, and MAPE = 5.93×10^{-5}.

It should be noted, all models with normalized output had the smallest RMSE compared with non-normalized output models. Also, proper normalization of the database accelerates training and could improve the accuracy of ANN models.

With the sensitivity analysis, it was shown that most variables influence the model. However, the input temperature is the variable that most influenced in addition to the variables that are related to the season of the year. The temperature at the tank of the feeding and the volumetric flow are variables that can be considered as possible opportunities to increase the outlet temperature.

Acknowledgments

The first, third, and fifth authors thank at CONACyT for the financial support received in the scholarships of the graduated students. The second author would like to thank the support provided by CONACyT: Cátedras CONACyT, under project No. 404.

Symbols

b_1	—	Bias in the hidden layer
b_2	—	Bias in the output layer

F	—	F-Fisher test
I_P	—	Importance of the input variable
LM	—	Levenberg–Marquardt training method
MAPE	—	Mean absolute percent error
n	—	Samples number
n_j	—	Network input term
P	—	Input variable
PTC	—	Parabolic trough collector
R^2	—	Coefficient of determination
RMSE	—	Root mean square error
S	—	Standard deviation combined
t	—	t-student test
T	—	Temperature (°C)
Wi	—	Weights
x	—	Value data
$\bar{x}$	—	Mean data
$\hat{x}$	—	Linear regression data
y	—	Value of interval normalization

Greek

δ	—	LOGSIG function
λ	—	PURELIN function
τ	—	TANSIG function

Subscript

amb	—	Ambient
exp	—	Experimental
feed	—	Feed/cold water tank
input	—	Fluid inlet
j	—	Neurons in the hidden layer
k	—	Neurons in the output layer
max	—	Value maximum
min	—	Value minimum
norm	—	Normalized
output	—	Fluid outlet
r	—	Neurons in the input layer
sim	—	Simulate
storage	—	Storage/hot water tank

References

[1] A. Sharif, S.A. Raza, I. Ozturk, S. Afshan, The dynamic relationship of renewable and nonrenewable energy consumption with carbon emission: a global study with the application of heterogeneous panel estimations, Renewable Energy 133 (2019) 685–691.

[2] H.A. Rypkema, Chapter 2.1 - Environmental chemistry, renewable energy, and global policy, Green Chem. (2018) 19–47, doi: 10.1016/B978-0-12-809270-5.00002-9.

[3] Y. Tian, C.Y. Zhao, A review of solar collectors and thermal energy storage in solar thermal applications, Appl. Energy, 104 (2013) 538–553.

[4] F. Jalili Jamshidian, S. Gorjian, M. Shafiee Far, An overview of solar thermal power generation systems, J. Sol. Energy Res., 3 (2018) 301–312.

[5] O.A. Jaramillo, M. Borunda, K.M. Velazquez-Lucho, M. Robles, Parabolic trough solar collector for low enthalpy processes: an analysis of the efficiency enhancement by using twisted tape inserts, Renewable Energy, 93 (2016) 125–141.

[6] V.K. Jebasingh, G.M. Joselin Herbert, A review of solar parabolic trough collector, Renewable Sustainable Energy Rev., 54 (2016) 1085–1091.

[7] T. Alam, M.H. Kim, A comprehensive review on single phase heat transfer enhancement techniques in heat exchanger applications, Renewable Sustainable Energy Rev., 81 (2018) 813–839.

[8] W.T. Ji, A.M. Jacobi, Y.L. He, W.Q. Tao, Summary and evaluation on single-phase heat transfer enhancement techniques of liquid laminar and turbulent pipe flow, Int. J. Heat Mass Transfer, 88 (2015) 735–754.

[9] W.T. Ji, A.M. Jacobi, Y.L. He, W.Q. Tao, Summary and evaluation on the heat transfer enhancement techniques of gas laminar and turbulent pipe flow, Int. J. Heat Mass Transfer, 111 (2017) 467–483.

[10] K. Bilen, M. Cetin, H. Gul, T. Balta, The investigation of groove geometry effect on heat transfer for internally grooved tubes, Appl. Therm. Eng., 29 (2009) 753–761.

[11] A.H. Elsheikh, S.W. Sharshir, M.A. Elaziz, A.E. Kabeel, W. Guilan, Z. Haiou, Modeling of solar energy systems using artificial neural network: a comprehensive review, Sol. Energy, 180 (2019) 622–639.

[12] E. Arce-Medina, J.I. Paz-Paredes, Artificial neural network modeling techniques applied to the hydrodesulfurization process, Math. Comput. Modell., 49 (2009) 207–214.

[13] S.A. Kalogirou, Artificial neural networks in renewable energy systems applications: a review, Renewable Sustainable Energy Rev., 5 (2001) 373–401.

[14] S.A. Kalogirou, Prediction of flat-plate collector performance parameters using artificial neural networks, Sol. Energy, 80 (2006) 248–259.

[15] A. Sözen, T. Menlik, S. Ünvar, Determination of efficiency of flat-plate solar collectors using neural network approach, Expert Syst. Appl., 35 (2008) 1533–1539.

[16] M. Caner, E. Gedik, A. Keçebaş, Investigation on thermal performance calculation of two type solar air collectors using artificial neural network, Expert Syst. Appl., 38 (2011) 1668–1674.

[17] S.Y. Heng, Y. Asako, T. Suwa, K. Nagasaka, Transient thermal prediction methodology for parabolic trough solar collector tube using artificial neural network, Renewable Energy, 131 (2019) 168–179.

[18] E.D. Reyes-Téllez, R.A. Conde-Gutiérrez, J.A. Hernández, E. Cardoso, S. Silva-Martínez, F. Z. Sierra, O. Cortés-Aburto, Optimal operating condition for a type W parabolic trough collector with low-cost components using inverse neural network and solved by genetic algorithm, Desal. Water Treat., 73 (2017) 80–89.

[19] O. May Tzuc, A. Bassam, M.A. Escalante-Soberanis, E. Venegas-Reyes, O.A. Jaramillo, L.J. Ricalde, E. Ordoñez, Y. El Hamzaoui, Modeling and optimization of a solar parabolic trough concentrator system using inverse artificial neural network, J. Renewable Sustainable Energy, 9 (2017) 013701-1–15, doi: 10.1063/1.4974778.

[20] Centro de Investigación en Ingeniería y Ciencias Aplicadas. Available at: http://www2.ciicap.uaem.mx/

[21] National Meteorological Service. Available at: https://smn.cna.gob.mx/ (query on October and November 2016).

[22] A. Parrales, D. Colorado, J.A. Díaz-Gómez, A. Huicochea, A. Álvarez, J.A. Hernández, New void fraction equations for two-phase flow in helical heat exchangers using artificial neural networks, Appl. Therm. Eng., 130 (2018) 149–160.

[23] M. Khayet, C. Cojocaru, Artificial neural network modeling and optimization of desalination by air gap membrane distillation, Sep. Purif. Technol., 86 (2012) 171–182.

[24] A.R. Khataee, M.B. Kasiri, Artificial neural networks modeling of contaminated water treatment processes by homogeneous and heterogeneous nanocatalysis, J. Mol. Catal. A: Chem., 331 (2010) 86–100.

[25] O.I. Abiodun, A. Jantan, A.E. Omolara, K.V. Dada, N.A. Mohamed, H. Arshad, State-of-the-art in artificial neural network applications: a survey, Heliyon, 4 (2018), doi: 10.1016/j.heliyon.2018.e00938.

[26] E. Martínez-Martínez, B.A. Escobedo-Trujillo, D. Colorado, L.I. Morales, A. Huicochea, J.A. Hernández, J. Siqueiros, Criteria for improving the traditional artificial neural network

methodology applied to predict COP for a heat transformer, Desal. Water Treat., 73 (2017) 90–100.
[27] D.E. Millán-Ocampo, A. Parrales-Bahena, J.G. González-Rodríguez, S. Silva-Martínez, J. Porcayo-Calderón, J.A. Hernández-Pérez, Modelling of behavior for inhibition corrosion of bronze using artificial neural network (ANN), Entropy, 20 (2018) 409.
[28] J. Han, M. Kamber, J. Pei, Data Mining Concepts and Techniques, 3rd Ed., Morgan Kaufmann Publishers 225 Wyman Street, Waltham, MA 02451, USA, 2012.
[29] A. Bassam, R.A. Conde-Gutierrez, J. Castillo, G. Laredo, J.A. Hernandez, Direct neural network modeling for separation of linear and branched paraffins by adsorption process for gasoline octane number improvement, Fuel, 124 (2014) 158–167.
[30] C.I. Rocabruno-Valdés, L.F. Ramírez-Verduzco, J.A. Hernández, Artificial neural network models to predict density, dynamic viscosity, and cetane number of biodiesel, Fuel, 147 (2015) 9–17.
[31] M. Mohanraj, S. Jayaraj, C. Muraleedharan, Applications of artificial neural networks for thermal analysis of heat exchangers - a review, Int. J. Therm. Sci., 90 (2015) 150–172.
[32] H.K. Ghritlahre, R.K. Prasad, Application of ANN technique to predict the performance of solar collector systems - a review, Renewable Sustainable Energy Rev., 84 (2018) 75–88.
[33] S.P. Verma, Estadística Básica para el Manejo de Datos Experimentales: Aplicación en la Geoquímica (Geoquimiometría), Universidad Nacional Autónoma de México, México Distrito Federal, 2005.
[34] S.P. Verma, R. Cruz-Huicochea, Alternative approach for precise and accurate Student´s t critical values and application in geosciences, J. Iberian Geol., 39 (2013) 31–56.
[35] J.A. Rodríguez, Y. El Hamzaoui, J.A. Hernández, J.C. García, J.E. Flores, A.L. Tejeda, The use of artificial neural network (ANN) for modeling the useful life of the failure assessment in blades of steam turbines, Eng. Fail. Anal., 35 (2013) 562–575.
[36] C.I. Rocabruno-Valdés, J.G. González-Rodriguez, Y. Díaz-Blanco, A.U. Juantorena, J.A. Muñoz-Ledo, Y. El-Hamzaoui, J.A. Hernández, Corrosion rate prediction for metals in biodiesel using artificial neural networks, Renewable Energy, 140 (2019) 592–601.
[37] A. Parrales, J.A. Hernández-Pérez, O. Flores, H. Hernandez, J.F. Gómez-Aguilar, R. Escobar-Jiménez, A. Huicochea, Heat transfer coefficients analysis in a helical double-pipe evaporator: nusselt number correlations through artificial neural networks, Entropy, 21 (2019) 689.
[38] J.A. Hernández, D. Colorado, Uncertainty analysis of COP prediction in a water purification system integrated into a heat transformer using several artificial neural networks, Desal. Water Treat., 51 (2013) 1443–1456.
[39] A. Mehta, A. Rawat, P. Chauhan, Advances in Electric Power and Energy Infrastructure, Proceedings of ICPCCI 2019, Vol. 608, Lecture Notes in Electrical Engineering (LNEE), 2020, p. 264.
[40] L.I. Morales, R.A. Conde-Gutierrez, J.A. Hernandez, A. Huicochea, D. Juarez-Romero, J. Siqueiros, Optimization of an absorption heat transformer with two-duplex components using inverse neural network and solved by genetic algorithm, Appl. Therm. Eng., 85 (2015) 322–333.